Structural deformation and mechanical response of CrS_2, $CrSe_2$ and Janus CrSSe

Shambhu Bhandari Sharma*[a], Ramesh Paudel[b], Rajendra Adhikari[c], Gopi Chandra Kaphle[d] and Durga Paudyal[e,f]

[a]Goldengate International College, Tribhuvan University, Kathmandu, Nepal
[b]Nepal Academy of Science and Technology, Khumaltar, Lalitpur, Nepal
[c]Department of Physics, Kathmandu University, Dhulikhel, Kavre, Nepal
[d]Central Department of Physics, Tribhuvan University, Kirtipur, Kathmandu, Nepal
[e]Ames Laboratory, Iowa State University, Ames, IA 50011 , USA
[f]Electrical and Computer Engineering,and Computer Science Departments, Iowa State University, Ames, IA 50011, USA

ARTICLE INFO

Keywords:
SIESTA
Janus TMD
Strain effects
Mechanical properties
Elastic isotropy

ABSTRACT

In the framework of density functional theory (DFT), we investigate the structural deformation, and mechanical behavior of the Janus CrSSe, which has out-of-plane structural asymmetry, with conventional transition metal dichalcogenides (TMDs) CrS_2 and $CrSe_2$. The Janus CrSSe could be a potential candidate for machinable optoelectronic and piezoelectric applications. We predict that these compounds are chemically, mechanically, and dynamically stable with the covalent bond between the TM(Cr) and chalcogen(X=S, Se) atoms. Due to the influence of tensile strain, the Cr-X bond length of each monolayers increases and the thickness decreases. Interestingly, the in-plane stiffness, shear and layer moduli, Poisson's ratio, ultimate bi/uni-axial stress of Janus CrSSe are in between the values of CrS_2 and $CrSe_2$ monolayers. Similar to TMDs, the orientation-dependent in-plane stiffness and Poisson's ratio demonstrates the isotropic behavior in Janus CrSSe. Furthermore, it can sustain a larger value of uni/bi-axial tensile strain with the critical strain equivalent to CrX_2 monolayers. By applying higher-order strain, we have also found average elastic-plastic behavior as expected. These findings demonstrate that the Janus CrSSe monolayer is a mechanically stable and ductile compound that maintains the hybrid behavior.

1. Introduction

The discovery of graphene[1] opens up the field of two-dimensional (2D) materials such as h-BN[2, 3, 4], SiC[5, 6], phosphorene[7], transitional metal dichalcogenides (TMDs)[8], and MXenes[9] for both theoretical and experimental research. These materials have drawn considerable interest due to their novel physical and chemical properties compared to their three-dimensional (3D) bulk counterparts. Depending upon the crystal structure, most of the TMDs exhibit substantial mechanical strength[10] with direct bandgap[11], higher carrier mobility[12, 13], and strong spin-orbit coupling (SOC)[14]. Unlike graphene and many other 2D materials, the in-plane asymmetry in TMDs provides them with extraordinary thermoelectric and optoelectronic properties[15, 16]. Particularly, chromium-based TMDs like CrS_2 and $CrSe_2$ show unique properties such as valley polarization in band structure[17], piezoelectric coupling, and phase-dependent intrinsic magnetic properties[18]. For example, a previous report shows that CrS_2 nanosheet has the potential to use as negative electrodes in lithium-ion batteries that could be promising for high-power energy storage[19]. Similarly, strain engineering has been implemented in the CrS_2 to modify the electronic, mechanical anisotropy, and piezoelectric behavior [20]. Moreover, reducing the dimension from 2D to 1D nanoribbon the electronic and magnetic behavior of CrS_2 changes significantly[21]. In addition, the thermal and mechanical properties of Cr-based TMDs are promising materials when they are engineered in heterostructure form [10]. Plus, the CrS_2 and $CrSe_2$ are two exceptional 2D valleytronic crystals with large valley spin splitting in the valence band[17].

Recently, a new derivative of TMDs, the so-called Janus TMD (JTMD) has drawn considerable interest due to their unique physical and chemical properties from the conventional TMDs because of an out-of-plane structural asymmetry. A single layer JTMD, MoSSe, was successfully fabricated in the laboratory by fully replacing the top Se layer of $MoSe_2$ TMD and inserting the S layer by using the chemical vaporization deposition (CVD) technique[22]. Further, several JTMDs have been studied theoretically[23, 24, 25, 26], which are mostly semiconductors with an energy bandgap between 1.36 to 1.97 eV exhibiting strong optical absorption at the visible region[27]. Particularly, the Janus chromium dichalcogenide monolayer (CrSSe) has broad optical absorption and low carrier recombination suitable for the photocatalytic system[28]. In addition, it shows better performance in photocatalytic reactions, water molecule absorptions, utilization of sunlight, charge separation and transport, and surface chemical reactions[29]. Similarly, 1T-phase of CrSSe JTMD possesses intrinsic 2D ferromagnetic behavior with

*Corresponding author
*Corresponding author
shambhubhandari789@gmail.com (S.B. Sharma*)
ORCID(s):

large spin- polarization and Curie temperature higher than the room temperature[30].

Although previous reports have verified that all 2H-phase group-VIB (in periodic table) TMDs are stable compounds, most of the studies are only focused on Mo-based and W-based dichalcogenides[20]. Recently, CrS_2 is successfully fabricated [18] but the experimental and theoretical understanding of many Cr-based TMD and JTMDs is still lacking. Many of their mechanical properties have not been investigated, in particular elastic-plastic behavior and critical tensile strength. Hence, the understanding of structural deformation and mechanical strength of JTMD CrSSe with its conventional TMD CrS_2 and $CrSe_2$ is critically important. The success will allow experimentalists to synthesize, characterize, and device these materials.

2. Computational details and structural information

We have used density functional theory (DFT) implemented in the Spanish initiative for electronic simulations with thousands of atoms (SIESTA) [31, 32]. The norm-conserving pseudopotentials in the semilocal form are used[33]. The generalized gradient approximation (GGA) functional with Perdew-Burke-Ernzerhof(PBE) [34] is adopted to treat underlying exchange and correlation within the double zeta plus polarization (DZP) basis sets. Brillouin zone integration has been performed using 15×15×1 Monkhrost pack [35] scheme. An energy cutoff of 350 Rydberg is used for the expansion of the reciprocal space. The atomic relaxation was achieved when the force reached the value of 0.02 eV/Å using the standard conjugate-gradient (CG) technique. The convergence criteria for the energy of the self-consistent field is set to be 1.0×10^{-6} eV. The vacuum gap of 25 Å is set along the z-direction to prevent unwanted interactions between the adjacent unit cells. The chemical stability is ensured by calculating and analyzing the formation (E_f) [36] and cohesive (E_{coh})[37] energies.

$$E_f = \frac{1}{3N}\left(E_{tot} - N(E_{Cr} + E_1 + E_2)\right)$$

$$E_{\text{coh}} = \left(E - \sum_{\text{i=Cr,S,Se}} n_{\text{i}} E_{\text{i}}\right)/N$$

where, E_{tot} is the total energy of monolayer structures, and E_{Cr} and E_1/E_2 are energies of Cr and S/Se atoms in their corresponding stable bulk phases with N number of atoms. In cohesive energy expression, E represents the total energy of a monolayer and E_i represents the total energy of isolated atoms with n_i as the number of a specific atom per monolayer. Further, we adopt the frozen phonon method implemented in the Vibra package of SIESTA for the calculation of phonon dispersion. We obtain an accurate force matrix with $5 \times 5 \times 1$ supercell for each monolayer.

The unit cell of monolayer TMDs CrS_2 and $CrSe_2$ consist of three atoms: one is transition metal (M = Cr) and another chalcogen (X = S or Se) atoms with MX_2 stoichiometry. These TMDs mainly exhibit three poly-type according to their atomic arrangement, namely, H - phase (hexagonal), T - phase (tetragonal), and T' - phase (distorted). Following the literature [17, 20, 38], we have chosen H-phase, which is energetically favorable among all these three phases. The hexagonal honeycomb CrX_2 structure consists of one Cr (bonded with 6 nearest X atoms) layer sandwiched between two S or Se atoms such that hexagonal symmetry can be seen from the top view. The X-M-X arrangement along the z-direction is considered a single layer, so-called TMD monolayer. Similarly, the hexagonal Janus CrSSe is formed by replacing one of X (S or Se) atoms layer from the 2H-CrX_2. In the Janus monolayer CrXY, the transition metal atom is bonded to three X atoms and three Y atoms. They possess reflection asymmetry on Cr-plane which leads to exhibit novel physical and chemical properties.

3. Results and Discussions

3.1. Structural properties

Following above mentioned structural information, we started our calculations by structural optimization after performing a careful convergence test. The same convergence criteria are met for all the monolayers. The optimized structure of the monolayer is shown in Fig. 1. The calculated values of lattice constants (a = b) for CrS_2, $CrSe_2$ and Janus CrSSe is 3.05, 3.23, and 3.14Å , respectively. The corresponding bond length between Cr-S and Cr-Se are 2.30 and 2.45 Å for CrS_2 and $CrSe_2$, respectively. Meanwhile, the bond length between Cr-S and Cr-Se in Janus CrSSe is 2.31 and 2.44 Å respectively. Similarly, the interlayer distance between two X atoms at the top layer and bottom layer gives the thickness (h) of the monolayer which are 2.97, 3.17, and 3.07 Å for CrS_2, $CrSe_2$ and Janus CrSSe monolayers, respectively. In addition, the bond angle between S-Cr-S, Se-Cr-Se, and S-Cr-Se in these respective monolayers are 80.31°, 80.71°, and 80.45°. The computed structural properties of all three monolayers are shown in Table 1, which are in good agreement with the available literature[20, 28, 38]. Our results demonstrate that the optimized lattice parameter, bond length, bond angle, and thickness are in the order of CrS_2< CrSSe< $CrSe_2$. The optimized values of the structural parameters of the Janus CrSSe monolayer are in between CrS_2 and $CrSe_2$ monlayers.

Further, to investigate the stability of the monolayers, the cohesive energy is calculated by using the above-mentioned relation in section 2. The calculated cohesive energies for CrS_2 , $CrSe_2$ and Janus CrSSe monolayers are -4.10, -3.59, and -3.83 eV, respectively. The lower value of cohesive energy indicates stronger interactions between the atoms in these monolayers. Hence, the structural stability is in the order of CrS_2>CrSSe>$CrSe_2$. The cohesive energy and the nature of the chemical bonding are closely related. Therefore, to analyze the nature of the bonding, we perform the Mulliken charge density calculations. The charge density contour plot (Fig. 2) shows that the charges are accumulated around the Cr atom in all the monolayers. Most of the

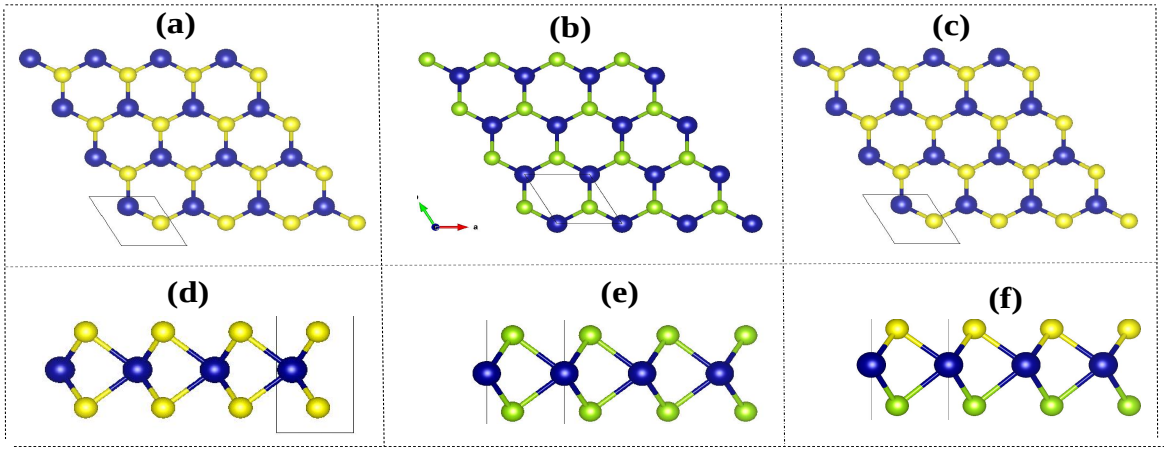

Figure 1: (Color online) Optimized monolayers: top and side views of CrS_2 (a, d), $CrSe_2$ (b, e) and Janus CrSSe (c, f). The blue, yellow, and green balls represent chromium, sulfur, and selenium atoms, respectively.

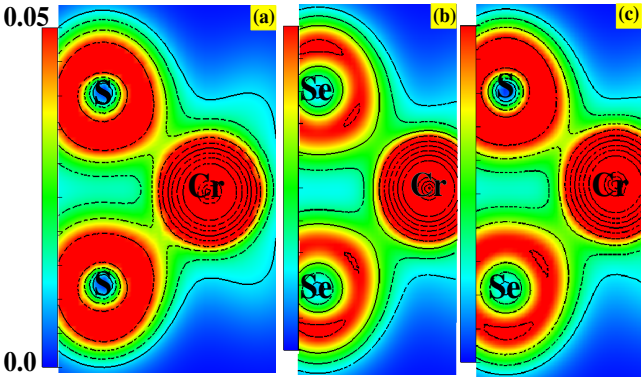

Figure 2: (Color online) Charge density countour plots of CrS_2 (a), $CrSe_2$(b), and the Janus CrSSe (c) monolayers, respectively.

valence charges are accumulated between Cr and S/Se atoms suggesting the covalent bonding between Cr-X/Y atoms.

To test the chemical stability of each monolayer, formation energy is calculated using the above mentioned relation in Section 2. The calculated formation energy of CrS_2, $CrSe_2$ and CrSSe monolayers are -1.7, -1.4 and -1.5 eV/atom, respectively. These computed values fairly agree with the available theoretical and experimental data. To test the dynamical stability of all monolayers, we have calculated phonon dispersion (Fig. 3) along with the Γ-K-M-Γ high-symmetry directions. The phonon dispersion bands depict the three acoustic and six optical bands due to the presence of bands from one Cr atom and two X (S or Se) atoms in the unit cell. The highest acoustic modes for the monolayers are in the order of CrS_2 > CrSSe > $CrSe_2$. In addition, the low-frequency gap between acoustic and optical modes in all the monolayers suggests the possibility of frequent scattering events[25]. The frequency and phonon dispersion bands of all three monolayers are not quite different from each other. The presence of real frequencies in all three monolayers demonstrates good dynamical stability.

After confirming the structural, chemical, and dynamical stabilities of the relaxed structures, it's crucial to test their response under the external strain. So, in the next section, we present the structural properties when external strain is loaded on all three monolayers.

3.2. Influence of strain in structural properties

To understand the deformation mechanism of each monolayer, we compute the variation of bond length as a function of strain. The 2D monolayers suffer geometrical changes due to tensile and compressive strain due to elongation and shrinking of bond lengths. There are two modes of strain loading that are physically meaningful for two-dimensional hexagonal symmetry, namely, uniaxial strain (ε_x or ε_y) and biaxial strain (ε_{xy}). The strain is loaded by varying the lattice constants within the elastic range. The uniaxial and biaxial strains are applied from -5% to +12% at the step of 2% to investigate the influences on the bond length and thickness of the monolayer.

First, we have investigated the strain energy response of each monolayer as a function of uniaxial and biaxial strain (Fig. 4 (d)). The response follows the parabolic path within the elastic range. The narrower and wider strain energy profiles are identified for CrS_2 and $CrSe_2$, respectively. Meanwhile, the Janus CrSSe is in between these two monolayers for both modes of strain. This analysis suggests that CrS_2 is the structurally most stable compound under the influence of strain as compared to other monolayers. The figure also proves that the minimum energy state of each monolayer is the strain-free equilibrium state. Additionally, the narrow strain energy curve in the biaxial strain as compared to the uniaxial strain indicates that the biaxial strain has a greater influence on the geometrical configuration. Furthermore, the variation of the bond length and thickness of the MLs are studied under the external strain is shown in Fig. 4(a-c). It is found that the bond length between the Cr and X (S or Se) atoms monotonically (small fluctuation in $CrSe_2$ at 2%) with an increase in tensile strain. Conversely, the bond length decreases with the increase of the compressive

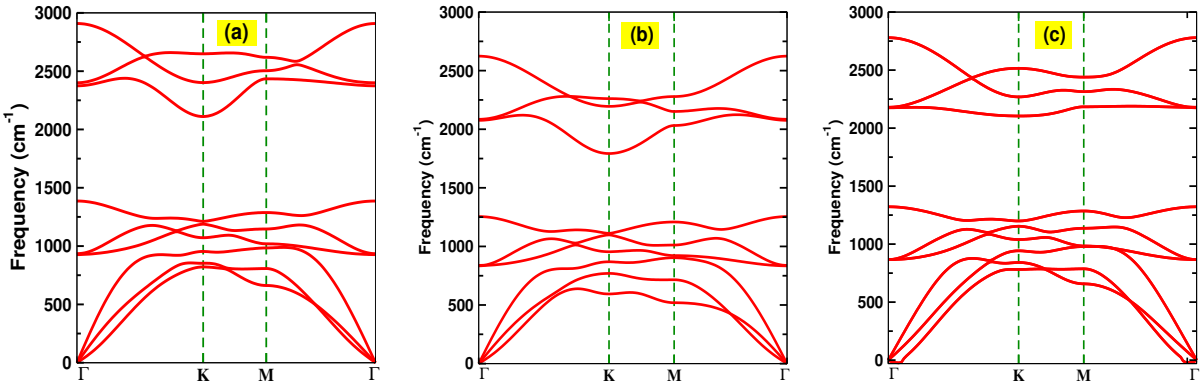

Figure 3: (Color online) Phonon dispersion bands of CrS_2 (a), $CrSe_2$ (b) and the Janus CrSSe (c) monolayers, respectively.

Table 1
Lattice parameters (a), bond length ($d_{Cr-X/Y}$), thickness (h), bond angle ($\measuredangle$) and, cohesive (E_c) and formation (E_f) energies of CrS_2, $CrSe_2$, and CrSSe monolayers.

Monolayers	a(Å)	$d_{Cr-X/Y}$(Å))	h (Å)	E_c(eV)	$\measuredangle X-M-X/Y$	$E_f(eV)$
CrS_2	3.05 3.04[39]	2.30 2.29[39]	2.97 2.95[38]	-4.10 -4.08[40]	80.31° 79.8°[39]	-1.59 -0.89[38]
$CrSe_2$	3.23 3.21[38]	2.45 2.38[41]	3.17 3.15[38]	-3.59 -	80.71° -	-0.96 -0.65[38]
CrSSe	3.14 3.13[36]	2.31,2.44 -	3.07 -	-3.83 -	80.46° -	-1.26 -1.79[36]

strain. Similarly, in the strain energy versus strain, the rate of variation of bond length is higher for biaxial strain. The bond length is found to be slightly sensitive towards the uniaxial strain for Janus CrSSe monolayer. This can be ascribed due to the difference in the S and Se atoms on the top and bottom layers. Plus, the difference in bond length and electronegativity may also play a role. The rate of variation of bond length is important to predict the structural strength of a system in external strain. To determine the rate of variation, we test the change of bond length at 12 %, which is within the elastic range. It is found that the rate of variation of Cr-X bond length is in the order of $CrSe_2$ >CrSSe > CrS_2. The smaller change in the bond length in CrS_2 indicates that it can withstand the larger tensile strain. On the other hand, the thickness of each monolayer decreases linearly with an increase in strain (small fluctuation in $CrSe_2$ at 2%). Conversely, the change in the thickness shows an opposite tendency, it becomes larger with respect to an increase in compressive strain.

Hence, it is clear that the bond length between Cr and S/Se increases with the decrease in thickness with the applied tensile strain. In this situation, the material tends to extend horizontally and compresses vertically. This is analogous to stretching a dough. This analysis shows that a significant geometrical transformation is created due to the applied strain as prescribed in ReXY (X=Y or X≠Y) where X=(S, Se) [42].

3.3. Mechanical properties

After realizing the effect of strain on structural properties, it is desirable to test the monolayer's mechanical strength and stability for their applications in nanomechanics. Considering this fact, we have made a comparative investigation of mechanical properties for all three monolayers. For 2D hexagonal symmetry, it is sufficient to find two main parameters such as Young's modulus and Poisson's ratio. The in-plane stiffness (C) is used as an alternative to Young's modulus because of reduced dimensionality. It measures the rigidity or flexibility of the material and it is defined as

$$C = \frac{1}{A_0}\frac{\partial^2 E_s}{\partial^2 \varepsilon},$$

where A_0, E_s , and ε are the area of strain-free monolayer, strain energy, and applied strain, respectively. On the other hand, the Poisson's ratio (ϑ) is defined as the ratio of the transverse strain to the axial strain and is expressed as $\vartheta = -\varepsilon_{\text{trans}}/\varepsilon_{\text{axial}}$. It is the mechanical response of a material to an applied uniaxial strain.

To calculate the mechanical parameters, the strain is applied in the x - axis (ε_x), y - axis (ε_y), and in both directions ($\varepsilon_x\varepsilon_y$) of the monolayer. The strain is applied from -2% to 2% for each direction with an increment of 1%. For each iteration of strain, the atomic positions of the system is fully relaxed. Further, the result is fitted to the strain energy, $E_s = a_1\varepsilon_x^2 + a_2\varepsilon_y^2 + a_3\varepsilon_x\varepsilon_y$ [43]. Here, a_1, a_2 and a_3 are three constants that are obtained during the

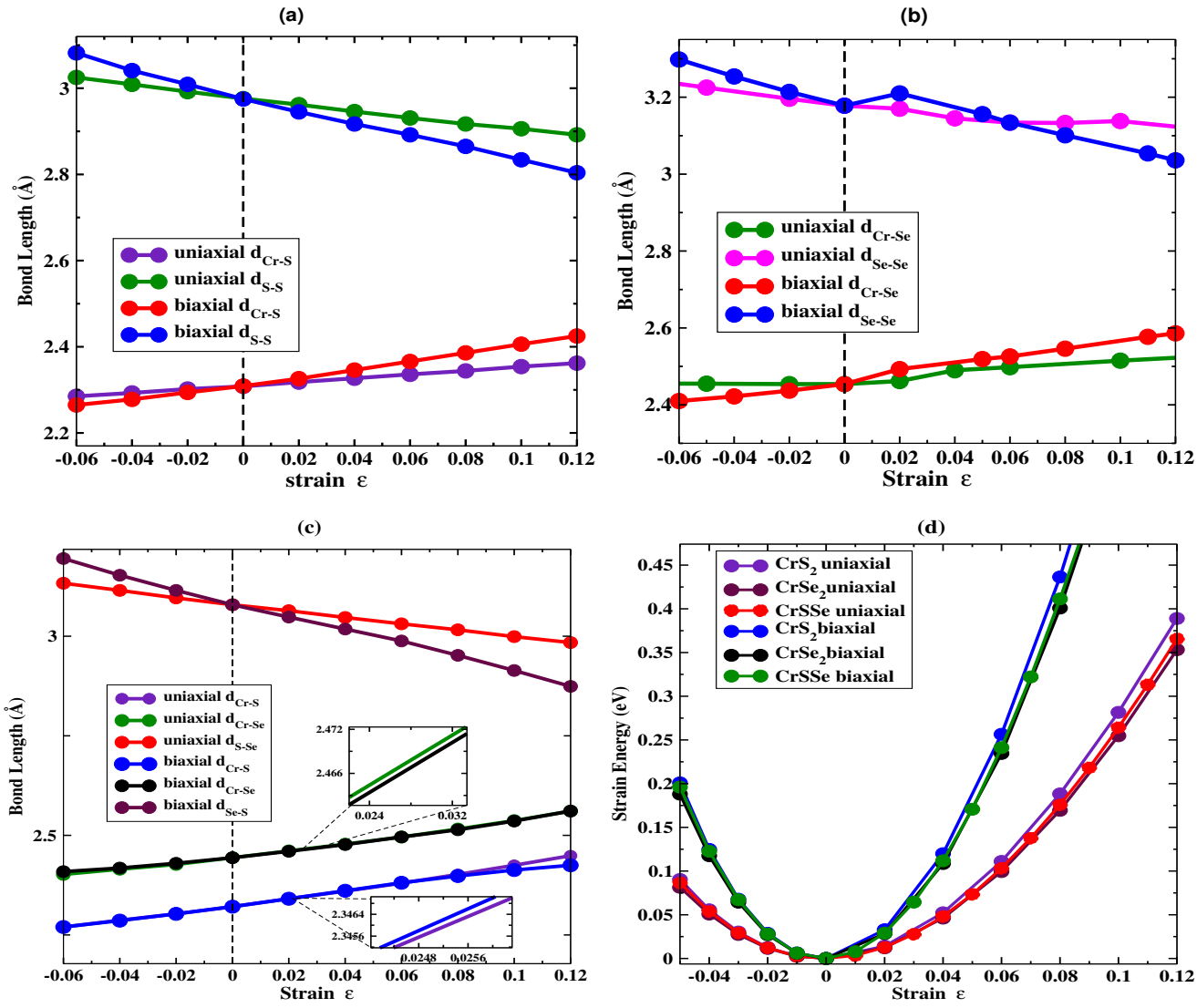

Figure 4: (Color online) The bond length with different thickness (a-c) and strain energy profile (d) as a function of uniaxial and biaxial strain for CrS_2, $CrSe_2$, and the Janus CrSSe monolayers, respectively.

fitting process. Further, due to the isotropy in the honeycomb symmetry, a_1 is equal to a_2. The three-dimensisonal surface fit (Fig. 5) shows the distribution of strain energy with respect to the different mode of applied strain. The strain energy profile of monolayers is in the order of $CrSe_2$ >CrSSe > CrS_2, which predicts the relative mechanical strength. The preceding expression is also obtained from elasticity matrix in terms of elastic stiffness constants C_{11} and C_{12} by employing $C_{11} = 2a_1/A_0$ and $C_{12} = a_3/A_0$. For hexagonal symmetry, C_{11} and C_{12} are only two significant independent elastic stiffness coefficients [44]. Another calculated elastic constant, C_{66} is (C_{11}-C_{12})/2. The in-plane stiffness (C) and Poisson's ratio(ϑ) are represented by $C_{11} \times [1 - (C_{12}/ C_{11})^2]$ and C_{12}/C_{11}, respectively. In 2D materials, the bulk modulus which gives a measure of the material's resilience to an external biaxial strain is calculated in terms of layer modulus (γ) with the expression, γ= (C_{11}+C_{22}+2C_{12})/4. In addition, using these second-order elastic constants C_{ij}, the shear modulus, K=C/2(1-ϑ), is calculated. The shear modulus estimates the resistance of a material to the shear strain. Further, the in-plane stiffness and Poisson's ratio are used to test the mechanical anisotropy. They are functions of the direction angles θ, which can be represented as [20]:

$$C(\theta) = \frac{C_{11}C_{22} - C_{12}^2}{C_{22}\cos^4(\theta) + A\cos^2(\theta)\sin^2(\theta) + C_{11}\cos^4(\theta)}$$
$$\vartheta(\theta) = \frac{C_{12}\cos^4(\theta) - B\cos^2(\theta)\sin^2(\theta) + C_{12}\cos^4(\theta)}{C_{22}\cos^4(\theta) + A\cos^2(\theta)\sin^2(\theta) + C_{11}\cos^4(\theta)} \quad (1)$$

where $A = \left(C_{11}C_{22} - C_{12}^2\right)/C_{66} - 2C_{12}$ and $B = C_{11} + C_{22} - \left(C_{11}C_{22} - C_{12}^2\right)/C_{66}$. The calculated values of C_{11} and C_{12} for all monolayers are shown in Fig. 6. Comparatively, the elastic constants are the highest for CrS_2 and the lowest for $CrSe_2$ with average value of the Janus CrSSe. The mechanical stability criteria [45] such as $|C_{11}| > |C_{12}|$ is fulfilled. The in-plane stiffness and Poisson's ratio follow

Table 2
The calculated elastic constants C_{ij}, in-plane stiffness C, and Poissons ratio ϑ, shear modulus K, and layer modulus γ for each monolayer

Monolayers	C_{ij} (N/m)		C(N/m)	ϑ	K(N/m)	γ(N/m)
	C_{11}	C_{12}				
CrS_2	118.73	31.41	110.42	0.26	43.66	75.06
Ref.[49]	120.44	31.66	112.12	0.26	-	-
$CrSe_2$	94.65	29.20	85.64	0.31	32.72	61.92
Ref.[49]	96.6	28.9	88.00	0.30	-	-
CrSSe	100.86	30.06	91.90	0.29	35.39	65.45
MoS_2 [a]	145	37	136	0.25	-	-
$MoSe_2$ [a]	116	33	106	0.29	-	-
MoSSe [a]	112	27	106	0.24	-	-

[a] Ref[46]

the same trend (Table 2). Interestingly, the stiffest monolayer CrS_2 (110.42 N/m) has the in-plane stiffness value closer to it's prototype MoS_2 (120.6 N/m [46]) but it is very much lower than that of graphene (370.1 N/m[47]). The physics behind the larger value of in-plane stiffness of CrS_2 is attributed to the highest value of cohesive energy per atom. In addition, the bond length between Cr and S is the lowest which holds creating the highest electrostatic pull that makes it much stiffer. Similarly, the larger values of Poisson's ratio of $CrSe_2$ and CrSSe indicate that these monolayers are more effective towards the uniaxial strain. For the same applied uniaxial strain, a longer contraction is found in the perpendicular direction. Further, the value of Poisson's ratio is the lowest for CrS_2 suggesting it as an effective material to resist the external shear force as compared to other monolayers. To confirm this fact, we evaluated the shear modulus for each monolayers (Table 2). The highest value of shear modulus for CrS_2 validates the result of Possion's ratio. In addition, the highest value of γ for CrS_2 suggests it as the most resilient monolayer for stretching.

The difference in in-plane stiffness and Poisson's ratio between the monolayers is attributed to the strength of the covalent bonding between chalcogen and transition metal atoms or due to the difference in electronegativity between the individual chalcogen atoms. In addition, the mechanical anisotropy is identified by fitting the polar plot of stiffness and Poisson's ratio relations. From the polar plot, (Fig. 7) the Poisson's ratio and in-plane stiffness for all monolayers are perfectly circular indicating elastically isotropic nature in agreement with the available literature [20, 48, 46]. With this analysis, we arrive in a conclusion that the in-plane stiffness and shear moduli rank in the same order as that of layer moduli revealing a relative hardness as also indicated in other TMDs and Janus monolayers.

3.4. Ultimate stress and strain

After confirming the mechanical stability and strength, we applied uniaxial and biaxial tensile strain with the increment of 2% until the monolayer is deformed. The stress as a function of uniaxial and biaxial tensile strain is shown in Fig. 8. The stress increases linearly with an increase in tensile strain within the harmonic range. Finally, the stress curve reaches the maximum value called ultimate tensile strength (U). The value of stress to achieve the ultimate strength is called ultimate stress. This is the maximum stress that a material can withstand without damaging itself. The critical stress also helps to separate the elastic and plastic regions of the material, which is discussed in Section 3.5. Below the ultimate stress higher order elastic constants are determined. There is a drop in stress indicating the system can not relax back to its equilibrium state because the maximum force barrier needs to be overcome. In this region, the material is in a metastable state ending with a fracture. The stress-strain curve shows that the ultimate stress in uniaxial strain (U_{uni}) is higher than that for biaxial strain (U_{bi}) in all three monolayers (Table 3). This result also supports the higher influence of the biaxial strain as mentioned above. In addition, the higher value of ultimate stress of CrS_2 indicates that a larger force is needed to break it as compared to other monolayers.

Table 3
The calculated ultimate stress (U) for uniaxial and biaxial tensile strain.

Monolayers	U_{uni} (N/m)	U_{bi} (N/m)
CrS_2	12.94 -	12.20 8.3[50]
$CrSe_2$	10.67 -	9.76 6.5[50]
CrSSe	11.51	10.17
MoS_2	-	15.00[51]

3.5. Elastic and plastic properties

We investigate the elastic and plastic behavior of the monolayer when tensile strain is applied to the larger value. The strain energy increases while increasing the strain within

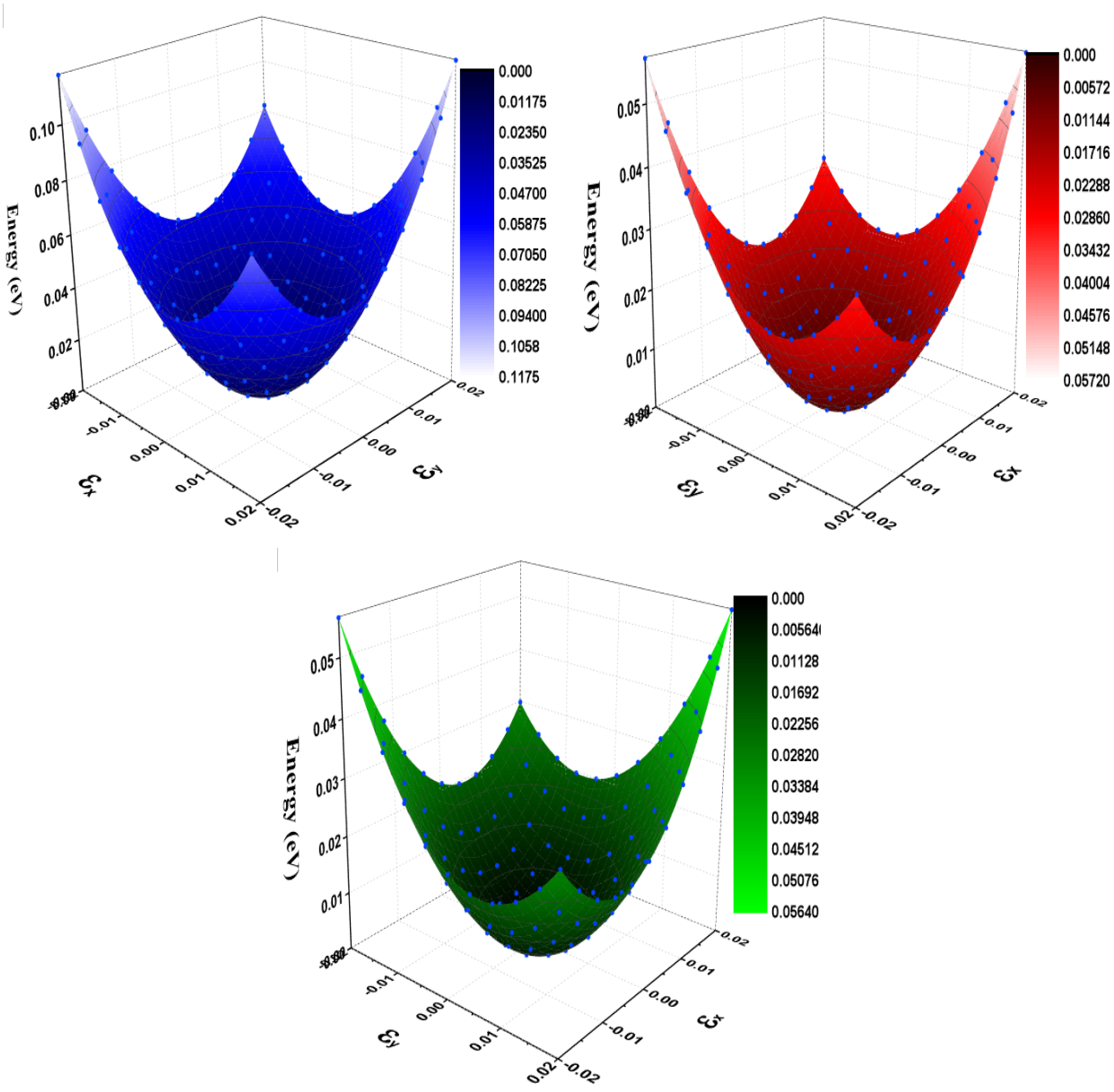

Figure 5: (Color online) Three-dimensional surface plots of strain energy versus strain for CrS_2 (blue), $CrSe_2$ (green) and the Janus CrSSe (red) monolayers.

the harmonic region (Fig. 9). The harmonic region indicates that even though the applied strain is removed the system relaxes back to its equilibrium state commonly known as the elastic region. Further, after reaching the maximum value (critical strain ε_c) the strain energy decreases beyond that the system transits from elastic to the plastic region (Fig. 9). The system in the plastic region will be in a metastable state. In this region, the removal of applied strain doesn't make it possible to relax back to its equilibrium geometry (irreversible structural change). Here, calculations show that the biaxial ε_c is significantly lower than that of the uniaxial ε_c (Table 4).

The higher ε_c of these materials suggest that they are ductile materials similar to MoS_2 [53].

The higher value of ε_c is attributed to the ability of the system to form the stable chemical arrangement between Cr atoms and S/Se atoms as also found in MoS_2 [51].

We note that our DFT computed values of U and ε_c are slightly higher than the previously estimated reference model [50] values. This discrepancy might be due to the methodology implemented in the calculations.

4. Conclusions

Here, we have investigated structural deformation and mechanical properties of CrSSe with traditional Cr-metal-based chalcogenides. Similar to the TMDs Janus CrSSe is a stable compound with covalent bond between the TM and chalcogen atoms. The reliably negative values of cohesive

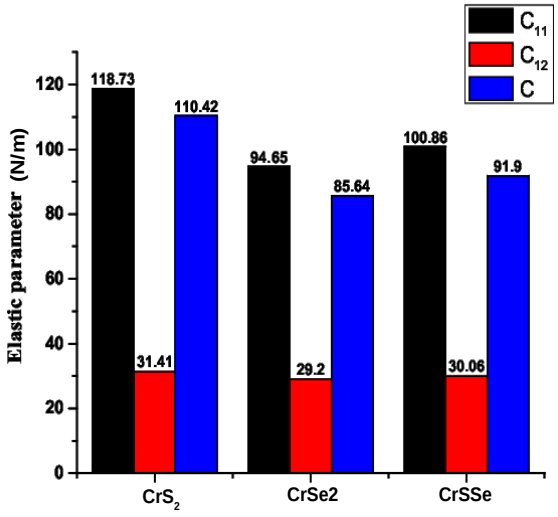

Figure 6: (Color online) Bar diagram comparing C_{ij} and in-plane stiffness of CrS_2, $CrSe_2$ and the Janus CrSSe monolayers.

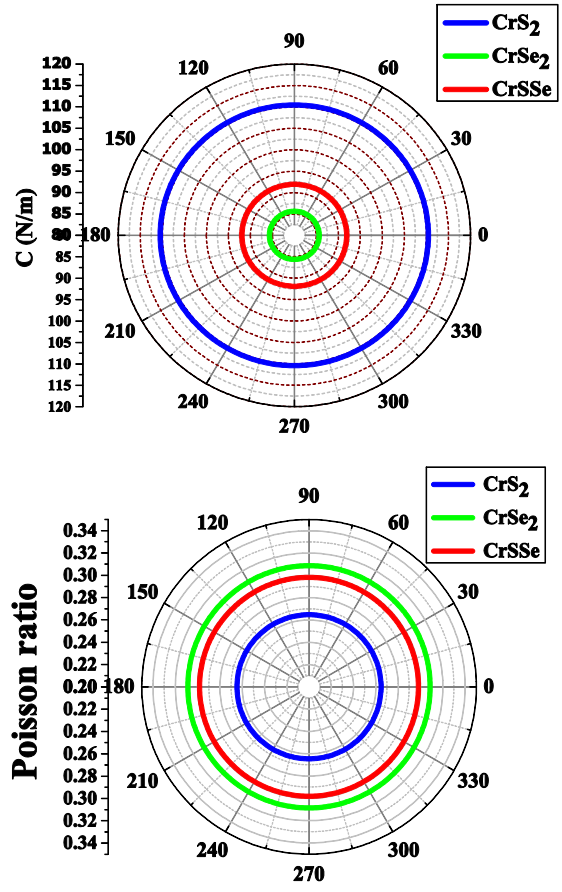

Figure 7: (Color online) The polar plots of orientation dependent in-plane stiffness and Poisson's ratio for CrS_2, $CrSe_2$ and the Janus CrSSe monolayers.

and formation energies confirm the chemical stability of these compounds. The influence of biaxial and uniaxial

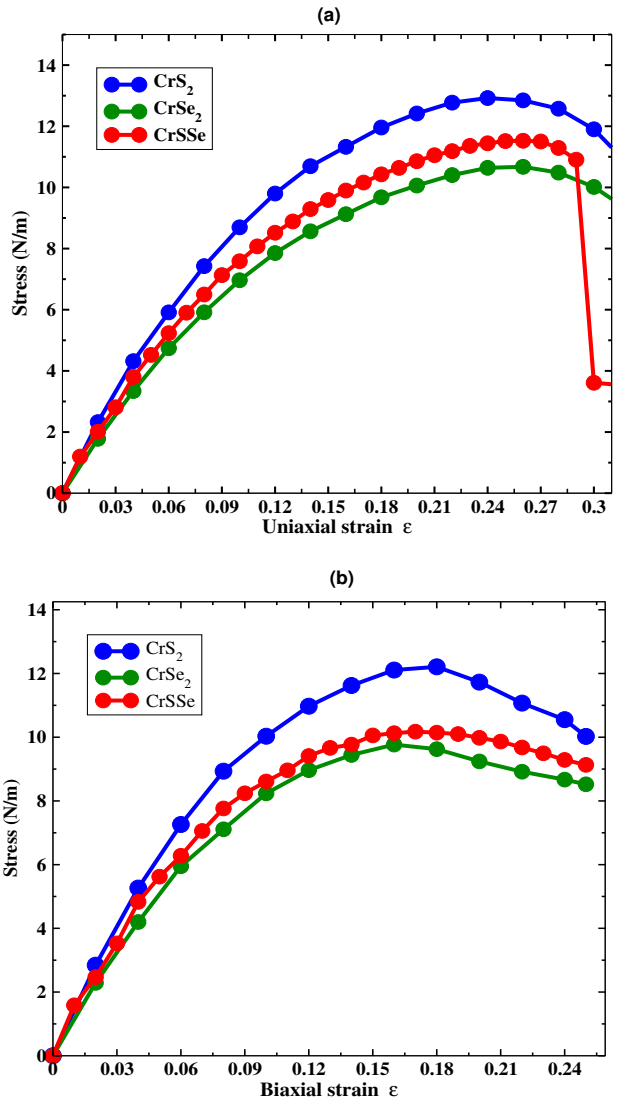

Figure 8: (Color online) The stress versus strain profile for CrS_2, $CrSe_2$, and the Janus CrSSe monolayers at uniaxial and biaxial strain.

Table 4
The critical elastic points (ε_c) for uniaxial and biaxial strains.

Monolayers	$\varepsilon_c(uniaxial)$	$\varepsilon_c(biaxial)$
CrS_2	0.24	0.18
$CrSe_2$	0.26	0.16
CrSSe	0.25	0.17
MoS_2	0.29 [52]	0.20[53]

strain increases the bond length between TM and Chalcogen atom whereas the thickness of monolayers decreases. Similarly, the bond angle between X-TM-X decreases due to the strain. The in-plane stiffness, shear and layer moduli, Poisson's ratio, ultimate bi/uni-axial stress of Janus CrSSe are in between the values of CrS_2 and $CrSe_2$ monolayers.

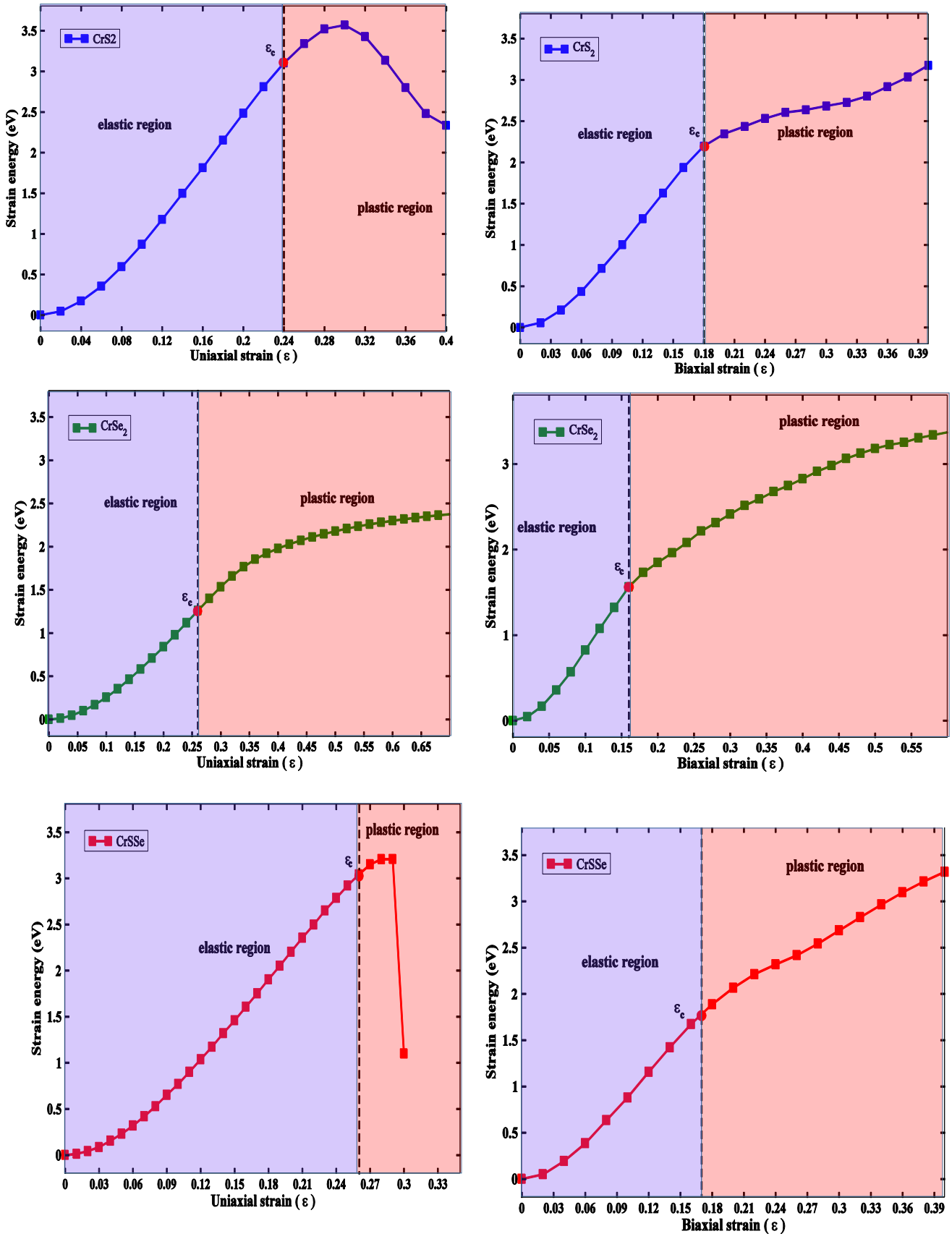

Figure 9: (Color online) Strain energy as a function of tensile biaxial and uniaxial strains. Here, ε_c (filled red circles) represents critical strains. The blue and pink colors divide the elastic and plastic regions.

This is due to the shorter bond length between Cr-S atoms resulting in the lowest cohesive energy in CrS_2.

Similar to TMDs, the orientation-dependent in-plane stiffness and Poisson's ratio indicates the isotropic behavior in Janus CrSSe. Furthermore, it can sustain a larger value of uni/bi-axial tensile strain with the critical strain equivalent to CrX_2 monolayers. In addition, it has the average elastic-plastic behavior. These findings demonstrate that the Janus CrSSe monolayer is a mechanically stable and ductile compound that maintains the hybrid character. These interesting results if validated from the experiment could bring the Janus CrSSe in optoelectronic and piezoelectric applications.

5. Acknowledgment

This research was supported in part through computational resources provided by the Kathmandu University Supercomputer Centre, which was established with equipment donated by CERN. We are very grateful to the Supercomputer Center (Kathmandu University) for providing high performance computing facilities during the research work. Work done at the Ames Laboratory was conducted for the US-DOE under it's Contract with Iowa State University, Contract No. DE-AC02-07CH11358.

CRediT authorship contribution statement

Shambhu Bhandari Sharma*: Conceptualization, Methodology, Software, Compilation of results, Original -manuscript writing. **Ramesh Paudel:** Group discussion, Manuscript- Reviewing and Editing. **Rajendra Adhikari:** Mentor, Simulation facilitator. **Gopi Chandra Kaphle:** Mentor, Group discussion, Manuscript- Reviewing and Editing. **Durga Paudyal:** Guidance, Manuscript- Reviewing and Editing .

References

[1] Kostya S. Novoselov, Andre K. Geim, Sergei Vladimirovich Morozov, Dingde Jiang, Michail I. Katsnelson, IVa Grigorieva, SVb Dubonos, Firsov, and AA. Two-dimensional gas of massless Dirac fermions in graphene. *nature*, 438(7065):197–200, 2005.

[2] Qing Peng, Wei Ji, and Suvranu De. Mechanical properties of the hexagonal boron nitride monolayer: Ab initio study. *Computational Materials Science*, 56:11–17, 2012.

[3] Li Song, Lijie Ci, Hao Lu, Pavel B. Sorokin, Chuanhong Jin, Jie Ni, Alexander G. Kvashnin, Dmitry G. Kvashnin, Jun Lou, Boris I. Yakobson, et al. Large scale growth and characterization of atomic hexagonal boron nitride layers. *Nano letters*, 10(8):3209–3215, 2010.

[4] Shambhu Bhandari Sharma, Ramchandra Bhatta, Keshav Raj Sigdel, Rajendra P Adhikari, and Gopi Chandra Kaphle. Structural, electronic, magnetic and mechanical properties of vanadium-doped boron nitride monolayer. *The European Physical Journal B*, 94(6):1–7, 2021.

[5] Zhiming Shi, Zhuhua Zhang, Alex Kutana, and Boris I. Yakobson. Predicting two-dimensional silicon carbide monolayers. *ACS nano*, 9 (10):9802–9809, 2015.

[6] Shambhu Bhandari Sharma, Rajendra Adhikari, Keshav Raj Sigdel, and Ramchandra Bhatta. Strain induced electronic and optical properties of 2d silicon carbide monolayer using density functional theory. *Journal of Nepal Physical Society*, 7(1):60–65, 2021.

[7] Saptarshi Das, Marcel Demarteau, and Andreas Roelofs. Ambipolar phosphorene field effect transistor. *ACS nano*, 8(11):11730–11738, 2014.

[8] Kin Fai Mak, Changgu Lee, James Hone, Jie Shan, and Tony F Heinz. Atomically thin mos 2: a new direct-gap semiconductor. *Physical review letters*, 105(13):136805, 2010.

[9] Jin-Cheng Lei, Xu Zhang, and Zhen Zhou. Recent advances in mxene: Preparation, properties, and applications. *Frontiers of Physics*, 10(3): 276–286, 2015.

[10] Deniz Çakır, Francois M Peeters, and Cem Sevik. Mechanical and thermal properties of h-mx2 (m= cr, mo, w; x= o, s, se, te) monolayers: A comparative study. *Applied Physics Letters*, 104(20): 203110, 2014.

[11] Jiang Pu and Taishi Takenobu. Monolayer transition metal dichalcogenides as light sources. *Advanced Materials*, 30(33):1707627, 2018.

[12] Se-Yang Kim, Jinsung Kwak, Cristian V Ciobanu, and Soon-Yong Kwon. Recent developments in controlled vapor-phase growth of 2d group 6 transition metal dichalcogenides. *Advanced Materials*, 31 (20):1804939, 2019.

[13] Se-Yang Kim, Jinsung Kwak, Cristian V Ciobanu, and Soon-Yong Kwon. Recent developments in controlled vapor-phase growth of 2d group 6 transition metal dichalcogenides. *Advanced Materials*, 31 (20):1804939, 2019.

[14] Wonbong Choi, Nitin Choudhary, Gang Hee Han, Juhong Park, Deji Akinwande, and Young Hee Lee. Recent development of two-dimensional transition metal dichalcogenides and their applications. *Materials Today*, 20(3):116–130, 2017.

[15] Kin Fai Mak and Jie Shan. Photonics and optoelectronics of 2d semiconductor transition metal dichalcogenides. *Nature Photonics*, 10(4):216–226, 2016.

[16] Ziliang Ye, Ting Cao, Kevin OâĂŹbrien, Hanyu Zhu, Xiaobo Yin, Yuan Wang, Steven G Louie, and Xiang Zhang. Probing excitonic dark states in single-layer tungsten disulphide. *Nature*, 513(7517): 214–218, 2014.

[17] Chengan Lei, Yandong Ma, Ting Zhang, Xilong Xu, Baibiao Huang, and Ying Dai. Valley polarization in monolayer crx2 (x= s, se) with magnetically doping and proximity coupling. *New Journal of Physics*, 22(3):033002, 2020.

[18] Mohammad Rezwan Habib, Shengping Wang, Weijia Wang, Han Xiao, Sk Md Obaidulla, Anabil Gayen, Yahya Khan, Hongzheng Chen, and Mingsheng Xu. Electronic properties of polymorphic two-dimensional layered chromium disulphide. *Nanoscale*, 11(42): 20123–20132, 2019.

[19] Eunjeong Yang, Hyunjun Ji, and Yousung Jung. Two-dimensional transition metal dichalcogenide monolayers as promising sodium ion battery anodes. *The Journal of Physical Chemistry C*, 119(47): 26374–26380, 2015.

[20] Shao-Bo Chen, Zhao-Yi Zeng, Xiang-Rong Chen, and Xing-Xing Yao. Strain-induced electronic structures, mechanical anisotropy, and piezoelectricity of transition-metal dichalcogenide monolayer crs2. *Journal of Applied Physics*, 128(12):125111, 2020.

[21] Anjna Devi, Arun Kumar, Amarjeet Singh, and PK Ahluwalia. A comparative spin dependent first principle study of monolayer (2d), armchair and zigzag nanoribbon (1d) of chromium disulfide (crs2). In *AIP Conference Proceedings*, volume 2265, page 030701. AIP Publishing LLC, 2020.

[22] Jing Zhang, Shuai Jia, Iskandar Kholmanov, Liang Dong, Dequan Er, Weibing Chen, Hua Guo, Zehua Jin, Vivek B Shenoy, Li Shi, et al. Janus monolayer transition-metal dichalcogenides. *ACS nano*, 11(8): 8192–8198, 2017.

[23] Wang-Li Tao, Yi Mu, Cui-E Hu, Yan Cheng, and Guang-Fu Ji. Electronic structure, optical properties, and phonon transport in janus monolayer ptsse via first-principles study. *Philosophical Magazine*, 99(8):1025–1040, 2019.

[24] Yi Yang, Yunzhen Zhang, Han Ye, Zhongyuan Yu, Yumin Liu, Bida Su, and Wenbin Xu. Structural and electronic properties of 2h phase janus transition metal dichalcogenide bilayers. *Superlattices and Microstructures*, 131:8–14, 2019.

[25] Wang-Li Tao, Jun-Qing Lan, Cui-E Hu, Yan Cheng, Jun Zhu, and Hua-Yun Geng. Thermoelectric properties of janus mxy (m= pd, pt; x, y= s, se, te) transition-metal dichalcogenide monolayers from first

principles. *Journal of Applied Physics*, 127(3):035101, 2020.

[26] Vuong Van Thanh, Nguyen Duy Van, Riichiro Saito, Nguyen Tuan Hung, et al. First-principles study of mechanical, electronic and optical properties of janus structure in transition metal dichalcogenides. *Applied Surface Science*, 526:146730, 2020.

[27] Jun Wang, Haibo Shu, Tianfeng Zhao, Pei Liang, Ning Wang, Dan Cao, and Xiaoshuang Chen. Intriguing electronic and optical properties of two-dimensional janus transition metal dichalcogenides. *Physical Chemistry Chemical Physics*, 20(27):18571–18578, 2018.

[28] Pei Zhao, Yan Liang, Yandong Ma, Baibiao Huang, and Ying Dai. Janus chromium dichalcogenide monolayers with low carrier recombination for photocatalytic overall water-splitting under infrared light. *The Journal of Physical Chemistry C*, 123(7):4186–4192, 2019.

[29] Lin Ju, Mei Bie, Jing Shang, Xiao Tang, and Liangzhi Kou. Janus transition metal dichalcogenides: A superior platform for photocatalytic water splitting. *Journal of Physics: Materials*, 3(2):022004, 2020.

[30] Junjie He and Shuo Li. Two-dimensional janus transition-metal dichalcogenides with intrinsic ferromagnetism and half-metallicity. *Computational Materials Science*, 152:151–157, 2018.

[31] José M Soler, Emilio Artacho, Julian D Gale, Alberto García, Javier Junquera, Pablo Ordejón, and Daniel Sánchez-Portal. The siesta method for ab initio order-n materials simulation. *Journal of Physics: Condensed Matter*, 14(11):2745, 2002.

[32] Emilio Artacho, Daniel Sánchez-Portal, Pablo Ordejón, Alberto Garcia, and José M Soler. Linear-scaling ab-initio calculations for large and complex systems. *physica status solidi (b)*, 215(1):809–817, 1999.

[33] Norman Troullier and José Luís Martins. Efficient pseudopotentials for plane-wave calculations. *Physical review B*, 43(3):1993, 1991.

[34] John P Perdew, Kieron Burke, and Matthias Ernzerhof. Generalized gradient approximation made simple. *Physical review letters*, 77(18): 3865, 1996.

[35] Hendrik J Monkhorst and James D Pack. Special points for brillouin-zone integrations. *Physical review B*, 13(12):5188, 1976.

[36] Pei Zhao, Yan Liang, Yandong Ma, Baibiao Huang, and Ying Dai. Janus chromium dichalcogenide monolayers with low carrier recombination for photocatalytic overall water-splitting under infrared light. *The Journal of Physical Chemistry C*, 123(7):4186–4192, 2019.

[37] Mohammad Noor-A-Alam, Hye Jung Kim, and Young-Han Shin. Dipolar polarization and piezoelectricity of a hexagonal boron nitride sheet decorated with hydrogen and fluorine. *Physical Chemistry Chemical Physics*, 16(14):6575–6582, 2014.

[38] Filip A Rasmussen and Kristian S Thygesen. Computational 2d materials database: electronic structure of transition-metal dichalcogenides and oxides. *The Journal of Physical Chemistry C*, 119(23): 13169–13183, 2015.

[39] Jianmin Zhang, Huiling Zheng, Ruilin Han, Xiaobo Du, and Yu Yan. Tuning magnetic properties of crs2 monolayer by doping transition metal and alkaline-earth atoms. *Journal of Alloys and Compounds*, 647:75–81, 2015.

[40] Xing-Hua Tian and Jian-Min Zhang. The electronic, magnetic and optical properties of single-layer crs2 with vacancy defects. *Journal of Magnetism and Magnetic Materials*, 487:165300, 2019.

[41] Can Ataca, Hasan Sahin, and Salim Ciraci. Stable, single-layer mx2 transition-metal oxides and dichalcogenides in a honeycomb-like structure. *The Journal of Physical Chemistry C*, 116(16):8983–8999, 2012.

[42] Jia-Qi Zong, Shu-Feng Zhang, Wei-Xiao Ji, Chang-Wen Zhang, Ping Li, and Pei-Ji Wang. Strain-mediated stability of structures and electronic properties of res2, janus resse, and rese2 monolayers. *Journal of Nanomaterials*, 2019, 2019.

[43] Mehmet Topsakal, Seymur Cahangirov, and Salim Ciraci. The response of mechanical and electronic properties of graphane to the elastic strain. *Applied Physics Letters*, 96(9):091912, 2010.

[44] Michael N Blonsky, Houlong L Zhuang, Arunima K Singh, and Richard G Hennig. Ab initio prediction of piezoelectricity in two-dimensional materials. *ACS nano*, 9(10):9885–9891, 2015.

[45] Max Born and Rama Dhar Misra. On the stability of crystal lattices. iv. In *Mathematical Proceedings of the Cambridge Philosophical Society*, volume 36, pages 466–478. Cambridge University Press, 1940.

[46] Wenwu Shi and Zhiguo Wang. Mechanical and electronic properties of janus monolayer transition metal dichalcogenides. *Journal of Physics: Condensed Matter*, 30(21):215301, 2018.

[47] Changgu Lee, Xiaoding Wei, Jeffrey W Kysar, and James Hone. Measurement of the elastic properties and intrinsic strength of monolayer graphene. *science*, 321(5887):385–388, 2008.

[48] M Yagmurcukardes, C Sevik, and FM Peeters. Electronic, vibrational, elastic, and piezoelectric properties of monolayer janus moste phases: A first-principles study. *Physical Review B*, 100(4):045415, 2019.

[49] Shao-Bo Chen, Zhao-Yi Zeng, Xiang-Rong Chen, and Xing-Xing Yao. Strain-induced electronic structures, mechanical anisotropy, and piezoelectricity of transition-metal dichalcogenide monolayer crs2. *Journal of Applied Physics*, 128(12):125111, 2020.

[50] Peter Hess. Predictive modeling of intrinsic strengths for several groups of chemically related monolayers by a reference model. *Physical Chemistry Chemical Physics*, 20(11):7604–7611, 2018.

[51] Simone Bertolazzi, Jacopo Brivio, and Andras Kis. Stretching and breaking of ultrathin mos2. *ACS nano*, 5(12):9703–9709, 2011.

[52] Junwen Li, Nikhil V Medhekar, and Vivek B Shenoy. Bonding charge density and ultimate strength of monolayer transition metal dichalcogenides. *The Journal of Physical Chemistry C*, 117(30): 15842–15848, 2013.

[53] M Yagmurcukardes, Ramazan Tuğrul Senger, François M Peeters, and H Sahin. Mechanical properties of monolayer gas and gase crystals. *Physical Review B*, 94(24):245407, 2016.